RSC Advances

ROYAL SOCIETY OF CHEMISTRY

www.rsc.org/advances

Evaluation of thermal stability and acoustic fingerprint spectra of energetic 1,2,4-triazoles based on bond lengths of chemical substituents using pulsed photoacoustic technique

K. S. Rao[a], A.K. Chaudhary[a,*], N. Kommu[a] and A.K. Sahoo[a,b]

[a] *Advanced Centre of Research in High Energy Materials, University of Hyderabad, Hyderabad-500 046, India*

[b] *School of Chemistry, University of Hyderabad, Hyderabad-500 046, India*

Email: anilphys@yahoo.com , akcphys@gmail.com

Abstract:

We investigated the effect of bond lengths of chemical substituents (attached to the para position of phenyl ring) on thermal stability of three newly synthesized nitro rich 1,2,4-triazoles named 1-(4-Methyl-3,5-dinitrophenyl)-1H-1,2,4-triazole (*P*-Me-DNPT),1-(4-Methoxy-3,5-dinitrophenyl)-1H-1,2,4-triazole (*P*-OMe-DNPT), 2,6-Dinitro-4-(1H-1,2,4-triazol-1-yl) aniline (*P*-NH_2-DNPT). The thermal stability of these compounds was evaluated along with their acoustic fingerprint spectra between 30 and 350 ^oC range, using pulsed photoacoustic (PA) pyrolysis technique. A 532 nm wavelength of 7 ns pulse duration and 10 Hz repetition rate, obtained from Q-switched Nd: YAG laser was used to determine the released NO_2 molecules during the process of thermal decomposition. The thermo gravimetric-differential thermal analysis (TG-DTA) data along with PA results highlights the multistep decomposition mechanism of 1,2,4-triazoles. The study also help us to distinguish the characteristic behavior of propellants and explosives of reported molecules as rocket fuel.

Keywords: 1,2,4-triazoles, Bond length, PA technique, Fingerprint, Thermal stability.

1. Introduction

Nitro rich tetrazoles, triazoles, pyrazoles and their derivatives are newly synthesized high energy materials (HEMs) which possess high heat of formation, detonation velocities, pressure, shock sensivity, and good thermal stability due to presence of aromatic ring [1-3]. The synthesis and characterisation of these HEMs molecules have attracted many researchers to evaluate their potential in milatary applications such as rocket fuel, gun propellants and explosives [4-10]. In addition, the study of thermal stability and decomposition mechanisms of premier HEMs moleules are reported by several research groups using different analytical techniques [11-15]. However, the photoacoustic (PA) technique is very versatile which offers several advantages such as high selectivity, sensitivity, fast response time and is also compact in size. As a result, it is widely used in trace gas detection between ppb to ppt level[16-20]. Further, the significance of PA signal is realised to monitor the released gaseous molecules from solid explosive available in small quantity (~1 mg) during the pyrolysis process. It is achieved by means of selection of proper excitation wavelength and designing of PA cell along with heating system. Therefore, the PA pyrolysis technique is one of the emerging analytical technique for the study of thermal decomposition and stability of newly synthesized HEMs molecules. In the present case, we have investigated the role of -NO_2, a major principal functional group on the thermal decomposition mechanism of compound in terms of strength of the PA signal and excited acoustic modes of the PA cavity. The released mechanism of gaseous molecules is accertained on the basis of bond length of the chemical substituent present in the compounds.

Kommu et al. reported the synthesis of these nitro rich 1,2,4-triazoles derivatives such as *P*-Me-DNPT, *P*-OMe-DNPT and *P*-NH_2-DNPT [21]. The structures along with the chemical formulas of these compounds are shown in Fig. 1. The phenyl ring of these compounds contains two NO_2 groups at their *meta* positions and the *para* position is occupied by methyl, methoxy and amino

groups, respectively. The estimated values of the densities (ρ), detonation velocities (D) of these compounds are 1.62, 1.64, 1.66 g/cm^3, and 6.40, 6.68, 6.66 km/s, respectively. The detonation velocity of *P*-OMe-DNPT has slightly higher value. This might be due to the presence of an additional O in –OCH_3 group. However, the stability of HEMs materials is strongly dependent on their molecular structure and bond lengths of chemical substituents present in the phenyl ring.

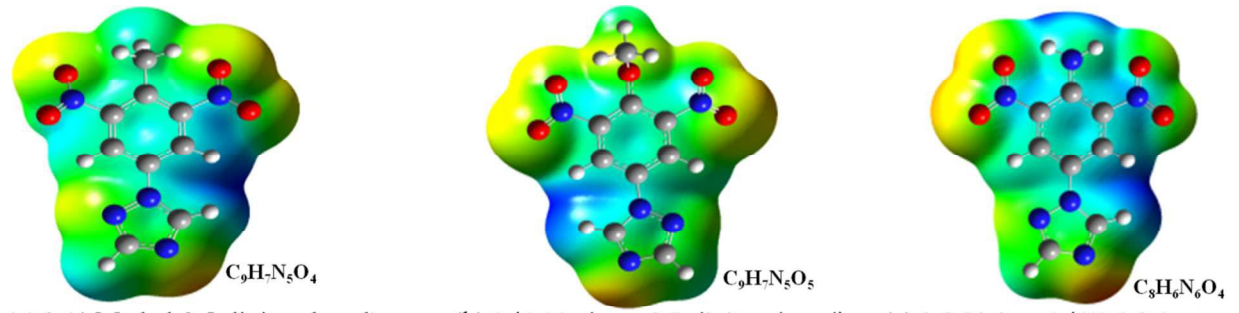

(a) 1-(4-Methyl-3,5-dinitrophenyl)-1H-1,2,4-triazole (*P*-Me-DNPT) (b) 1-(4-Methoxy-3,5-dinitrophenyl)-1H-1,2,4-triazole (*P*-OMe-DNPT) (c) 2,6-Dinitro-4-(1H-1,2,4-triazol-1-yl) aniline (*P*-NH_2-DNPT)

Fig. 1 Structure of the compounds.

The reported energetic 1,2,4-triazoles compounds can be used as an explosive and as propellants. We know that explosives and propellants generate supersonic and subsonic reaction waves, respectively, which propagate with a speed of several km/s, inside the matter, accompanied with hot gases. This process is known as detonation and deflagration, respectively [22]. Thermal stability and the efficiency of these compounds as a rocket fuel are ascertained on the basis of strength of the PA signal produced due to absorption of released NO_2 molecules during the process of decomposition. In the present case, -NH_2 group increases the efficiency of compound. The TG-DTA graph provides the information about the melting and decomposition temperatures and the residual weight of the compound. The PA study also helps to differentiate the compounds based on PA spectra produced due to absorption of 532 nm wavelength.

2. Theory and Experimental Details:

The wave equation of the sound pressure for the inhomogeneous medium in the lossless cylindrical resonator can be illustrated by [23-26]

$$\frac{d^2P(r,t)}{dt^2} - c^2\nabla^2 P(r,t) = (\gamma - 1)\frac{dH(r,t)}{dt} \quad (1)$$

Where, c is the sound velocity, γ is adiabatic coefficient of the gas and H is the heat density stored by light absorption. The solution of Eq. (1) is given by the following equation:

$$P(r,t) = \sum_{n=0}^{\infty} A_{n,m}\, e^{im\omega_o t} P_n(r) \quad (2)$$

The dimension less eigenmodes distribution of cylindrical resonator is the solution of the homogeneous wave equations, which can be expressed as:

$$P_n(r,t) = P_n(r)e^{i\omega_n t} \quad (3)$$

Where, ω_n is the resonance frequency of the cavity resonator and $P_n(r)$ is given by

$$P_n(r) = P_{mnq}(r,\emptyset,z) = J_m(K_r r)\cos(K_z z)\begin{pmatrix}\cos(m\emptyset)\\ \sin(m\emptyset)\end{pmatrix}\pi r^2 \quad (4)$$

The amplitude (A_n) of the PA signal for pulsed laser is proportional to the deposited heat density which directly depends on input laser power (E) [27,28]

$$A_n = \frac{(\gamma-1)\, L\, f_n\, P_n(r_m)\, \alpha\, E}{V} \quad (5)$$

Where, f_n is the normalized overlap integral that describes the effect of the spatial overlap between the propagating laser beam and the pressure distribution of the n^{th} acoustic eigenmodes. L, V are the length and volume of the PA cell, respectively. α is the PA absorption coefficient of the sample and, γ is the adiabatic constant of the buffer gas. The PA cell has three types of excited acoustic modes i.e. longitudinal (q), radial (n) and azimuthal (m) acoustic modes. The

frequency of the acoustic resonant modes generated within the cylindrical type PA cavity is described as

$$F_{mnq} = \frac{c}{2}\left(\left(\frac{\alpha_{mn}}{R}\right)^2 + \left(\frac{q}{L}\right)^2\right)^{1/2} \quad (6)$$

Where c, R and L are the sound velocity, radius and length of the cylindrical resonator, respectively. α_{mn} is the n^{th} zero of the derivative of the m^{th} Bessel function at $r = R$. The PA spectrum was recorded using a PA cell made of stainless steel with internal diameter of 1.5 cm and length of 7.5 cm.

The experimental design is shown in Fig. 2. A Q-switched Nd: YAG laser (Model Spit, Germany) of wavelength 532 nm, pulse duration 7 ns and repetition rate 10 Hz was used to excite the vapor of the compounds in a cylindrical PA cavity. The laser beam diameter was adjusted to 6 mm using aperture and allowed to pass through the centre of the PA cavity. The generated PA signal was detected by a pre-polarized microphone of responsivity 50 mV/Pa (BSWA, China), which was housed in the centre of PA cell. The output signal of the microphone was fed to the preamplifier coupled to a 200 MHz oscilloscope (Tektronix, U.S.A.). The analysis was carried out using data acquisition program, which was developed using LabView software.

The solid compound of small quantity (~ 1 mg) is kept in a specially designed heating system, which facilitates the controlled pyrolysis between 30 and 350 ^{o}C range. The entire system was evacuated upto 10^{-2} Torr using a rotating vacuum pump. The released vapor of the solid compound at required temperature was introduced to PA cell for recording of PA spectrum at desired incident laser energy (E_{in}) and data acquisition time (t). The energy of the incident laser pulse was measured with power meter (EPM2000, Coherent).

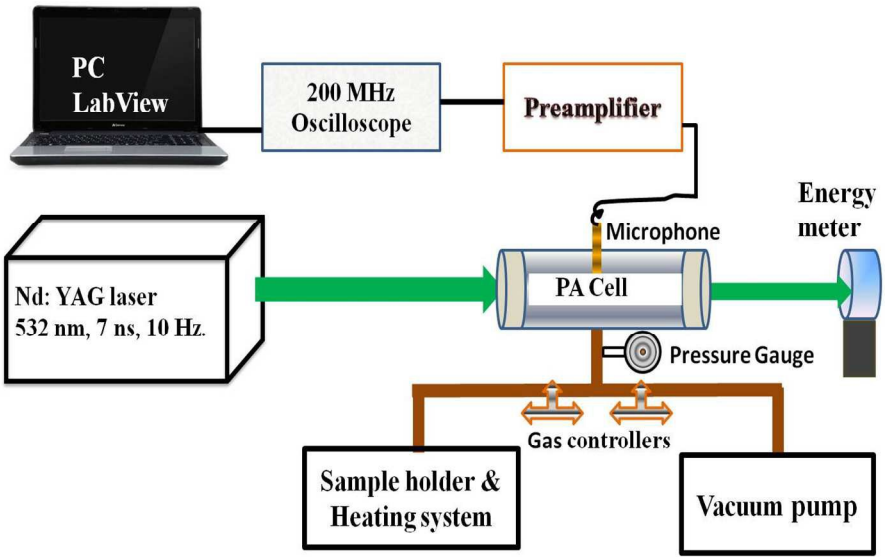

Fig. 2 Experimental set up.

Thermo gravimetric-differential thermal analysis (TG-DTA) was carried out using TA instrument (Model No. Q600DT). The TG-DTA analysis has been conducted with initial weights 1.589 mg of *P*-Me-DNPT, 1.002 mg of *P*-OMe-DNPT, and 3.254 mg of *P*-NH_2-DNPT, respectively. The solid compound was introduced into an alumina crucible and heated between 25-400 ^oC range under nitrogen gas atmosphere (flow rate of 100 cm^3 / min) which works as the purge and protective gas. An empty alumina crucible was used as reference. Non-isothermal TGA runs were conducted between 25-400 ^oC ranges at nitrogen atmosphere with purge rate of 10 ^oC/min. In addition, infrared spectra of these compounds were recorded using Perkin-Elmer IR spectrometer in 400-4000 cm^{-1} range in form of KBr pellets.

3. Results and Discussions

3.1. IR spectra of compounds

Fig. 3(a-c) shows the IR spectra of *P*-Me-DNPT, *P*-OMe-DNPT, and *P*-NH_2-DNPT respectively. Inset tables of Fig. 3 shows the structural positions of principal functional groups present in the compound. The absorption peaks of amino group are present at 3419.18 , 3254.79 and 1649.32 cm^{-1}, respectively. The strongest absorption peaks of C-O-C, -NO_2, –N=N^+=N^- , -OCH_3 and C-H

are observed between 1300-1000 cm^{-1}, 1550-1300 cm^{-1}, 2400-2000 cm^{-1} and 2850-2810 cm^{-1}, range respectively. Therefore, the provided FTIR spectra confirms the presence of different functional groups in the reported compounds.

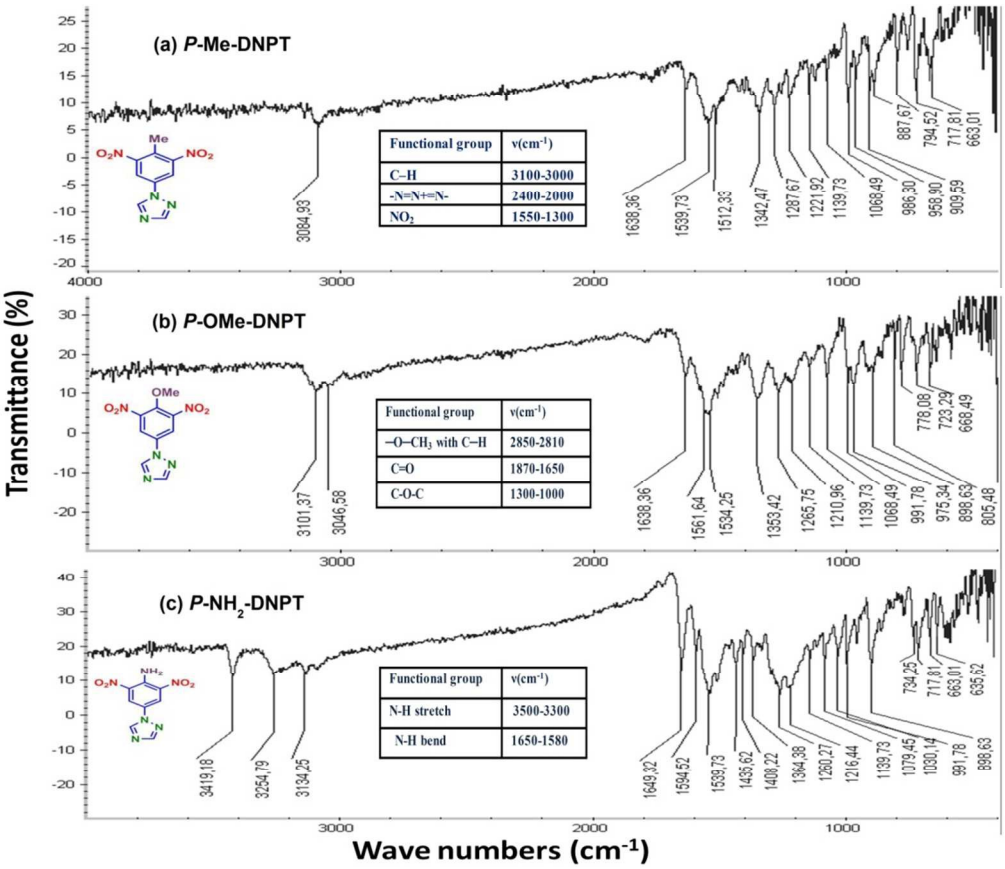

Fig. 3 IR spectra of solid compounds.

3.2. Thermal PA fingerprint spectra of compounds

Fig. 4(a-c) shows the thermal PA spectra of *P*-Me-DNPT, *P*-OMe-DNPT and *P*-NH_2-DNPT, respectively. The PA spectra was recorded at incident laser energy E_{in} = 8.63 mJ and data acquisition time t = 0.5 ms.

Fig. 4(a) shows that *P*-Me-DNPT does not provide any PA signal upto 60 ^oC. The first PA signal is observed at 90 ^oC, which is treated as an initial point of thermal decomposition. The PA spectra also shows some sharp intense acoustic modes located at 12.4 and 36.4 kHz. In addition,

the other excited acoustic modes appear in cluster form and occupy the range between 16 and 35 kHz. The excited acoustic modes of the PA cavity at T_d = 250 ^{o}C are present at 3.2, 8.4, 12.4, 18, 20.8, 22, 23.2, 27.4, 32.2, 36.4, 42.2 and 44.2 kHz respectively. The PA mode present at 12.4 kHz is one of the predominant acoustic mode of the cavity and has intensity of the order of 54.11 mV. It is observed that acoustic modes of thermal PA spectra of the compound has ± 200 Hz variation with respect to their central frequency. The background noise signal of the system is of the order of 0.05 mV.

Fig. 4(b) shows the thermal PA spectra of *P*-OMe-DNPT. Though its melting temperature (T_m) is 97.92 ^{o}C, the process of dissociation initiates at 30 ^{o}C. Therefore, once again it is confirmed that the NO_2 molecules are released much before the melting temperature of the HEMs compounds [29,30]. The majority of acoustic modes exhibit cluster behavior and have broad profiles due to the change in the density of released vapor. The sharp intense peaks are only located at 3.8 and 13.8 kHz between 30-350 ^{o}C range. However, the other higher intensity acoustic modes are present at 17.2, 22 and 35.8 kHz, respectively. It is observed that almost all acoustic modes of PA spectra are excited simultaneously and possess identical intensities. Since, the PA spectra of the compound is generated due to absorption of incident laser radiation by NO_2 and the presence of other gaseous molecules (released due to methoxy group) lead to change the density of the cell medium which affects the velocity of acoustic pressure waves. As a result, the profile of acoustic modes shows broadening effect along with shift in the frequency with respect to the central frequency. The predominant order of excited acoustic modes gradually change their position with respect to vapor temperature.

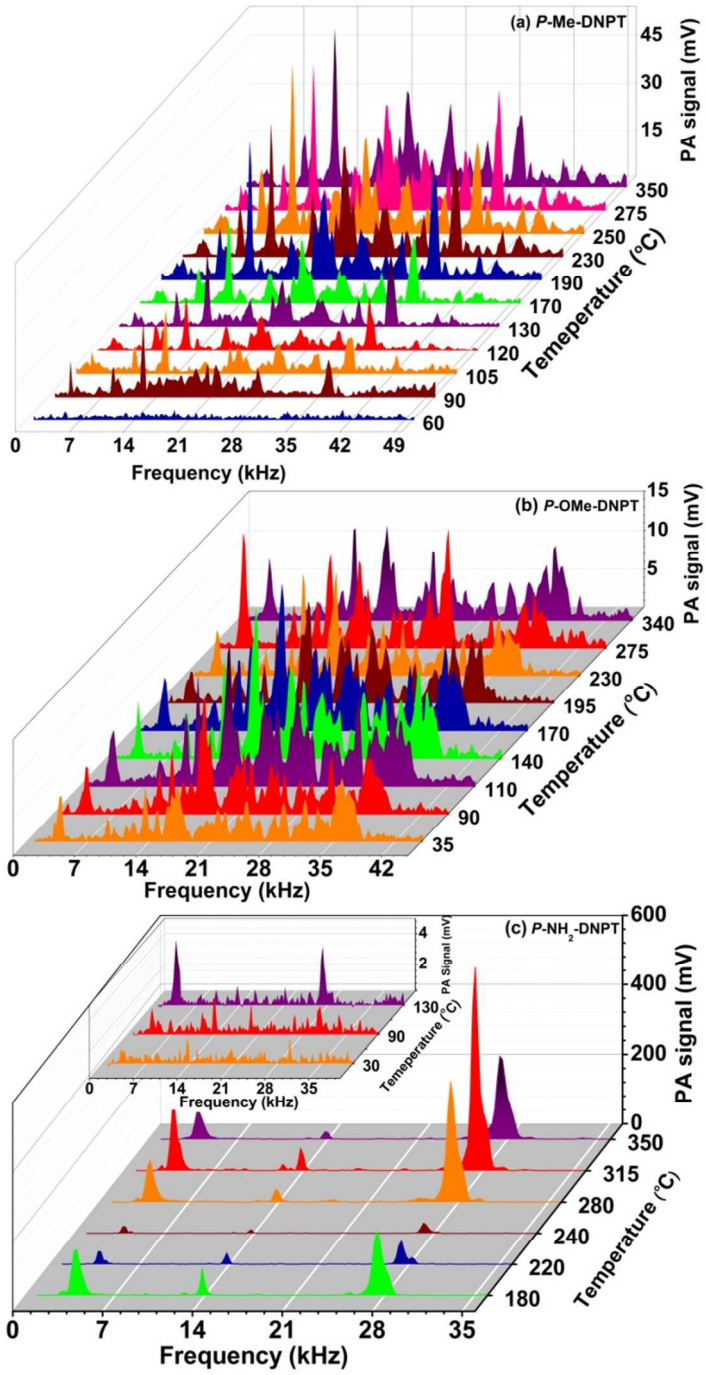

Fig. 4 Thermal PA spectra of three compounds.

Fig. 4(c) shows the thermal PA spectra of *P*-NH_2-DNPT. The compound shows two weak and one strong mode at 130 ^{o}C, which are present at 4.0,13.8 and 27.4 kHz respectively. This compound releases more quantity of NO_2 molecules as compared to other compounds. Consequently, the PA spectra has strong and sharp acoustic peaks. The maximum PA signal is

obtained at 315 ^{o}C and the excited acoustic modes are located at 4, 12.4, 13.8, 27.4, 37.6 ,38.6 and 39.11 kHz, respectively. During the experiment, thermally released redish brown colored vapor was observed in the heating flask, which clearlly indicates that the vapor contains high quantity of NO_2 as compared to other gaseous molecules.

Fig. 5(a-c) shows the PA fingerprint spectra of compounds. Inset figures shows the corresponding time domain signals. The PA spectra is recorded at 250, 170 and 280 ^{o}C at t = 1 ms for *P*-Me-DNPT, *P*-OMe-DNPT and *P*-NH_2-DNPT, respectively. Fig. 5(d) shows the total number of 24 calculated eigenmodes which comprises 19-longitudinal, 3-radial and 2-azimuthal modes of the PA cavity, which occupies the frequency between 0-45 kHz. The first q, n and m modes frequencies are located at 2.28,13.4 and 27.89 kHz, respectively. The calculated values of sixth and twelfth longitudinal modes are almost equal to the first radial and azimuthal modes, respectively. It is inferred that these common eigenmodes are the strongest excited acoustic modes of PA spectra of the sample, it is clearlly observed in PA spectra of *P*-NH_2-DNPT. The sixth longitudinal and first radial modes have equally occupied the position at 13.8 kHz. Similarly, the twelfth longitudinal mode coincided with the first azimuthal mode and is present at 27.4 kHz. The PA cavity have maximum numbers of even order longitudinal modes. Since, the strength of PA signal and order of excited acoustic mode varies from compound to compound and is attributed to the change in the density of released gaseous molecules.

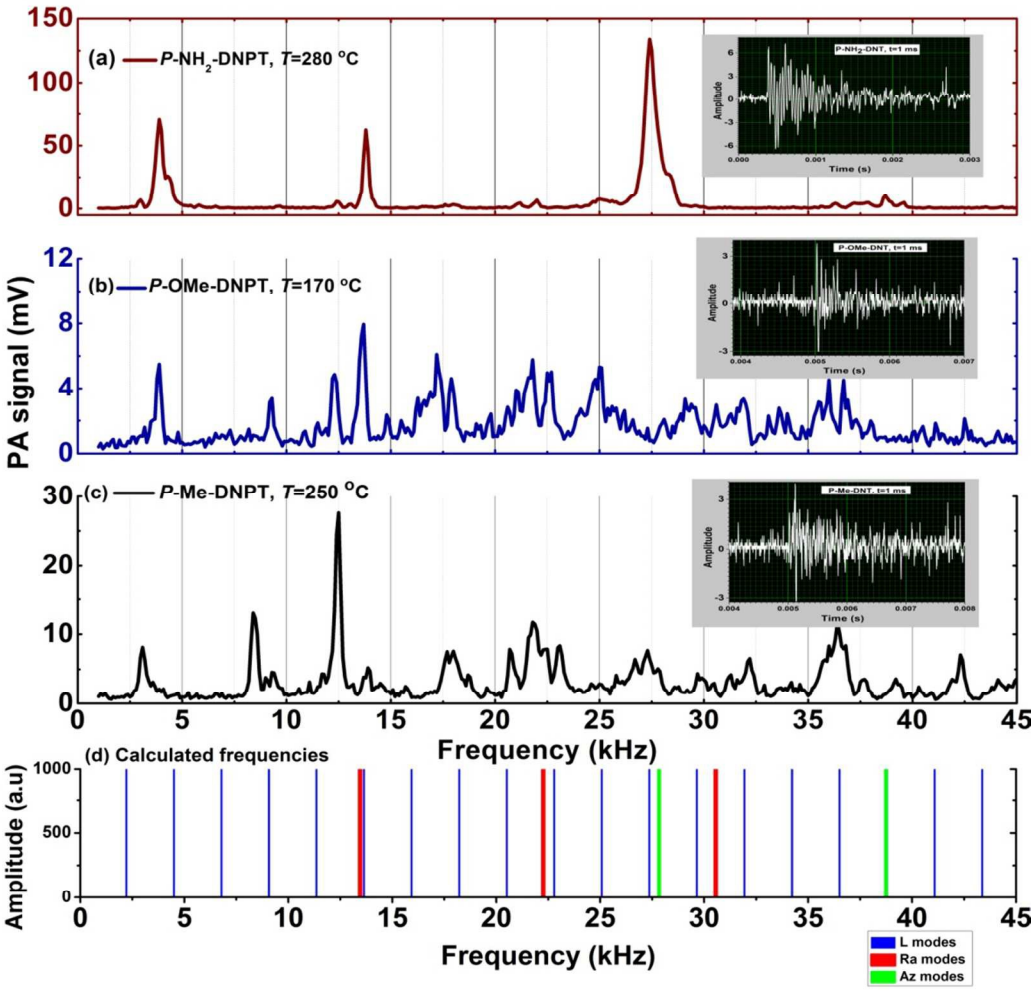

Fig. 5. PA fingerprint spectra at t =1 ms of (a) *P*-NH_2-DNPT (b) *P*-OMe-DNPT (c) *P*-Me-DNPT, and (d) calculated longitudinal, radail and azimuthal modes of PA cavity.

In case of PA spectra of *P*-Me-DNPT and *P*-OMe-DNPT, the acoustic modes are well seperated and have sharp peaks between 0-15 kHz frequency range. Whereas, low intensity acoustic modes appeared in pair between 15-45 kHz range. It confirms that the higher order modes are forming clusters due to percentile change of NO_2 as well as other gaseous molecules present in the vapor. However, PA spectra of *P*-NH_2-DNPT has two kinks at 4.4 and 28.3 kHz. The PA spectra of *P*-NH_2-DNPT depicts well seperated sharp peaks compared to other two compounds and confirms that *P*-NH_2-DNPT releases more quantity of NO_2 as compared to other byproduct gases. While, the kinks of acousitc modes show the presence of other gaseous molecules released in less quantity.

In our previous report, we have shown the thermal stability and acoustic fingerprints of several new compounds such as 1-(2,4-dinitrobenzyl)-1H-1,2,3-triazole (S_1), 1-(3,5-dinitrobenzyl)-1H-1,2,3-triazole (S_2), 1-(2-methoxy-3,5-dinitrobenzyl)-1H-1,2,3-triazole (S_3), 1-(4-methoxy-3,5-dinitrobenzyl)-1H-1,2,3-triazole (S_4) [31]. The effect of methoxy group on PA spectra of S_3 and S_4 is observed in form of pairs. Additional acoustic peaks are absent in the PA spectra of S_1 and S_2. Similarly, *P*-OMe-DNPT also possess pair of acoustic peaks. The variation in the density of gaseous fragments is due to the presence of -OCH_3 group, as a result the intensity of acoustic modes is comparatively lower than the remaining two compounds.

The thermally released gases such as oxygen (O) or CO from methoxy group, might react with freely released NO_2 molecules and leads to convert NO_2 to NO with formation of other gases such as O_2 and CO_2 etc. using following chemical root [32,33]

$$NO_2+O\rightarrow NO+O_2 \quad (2)$$

$$NO_2+CO \rightarrow NO+CO_2 \quad (3)$$

3.3. Thermal stability of compounds

Fig. 6(a, c and e) shows the behavior of acoustic modes with respect to temperature while Fig. 6(b, d and f) shows TG-DTA thermo graphs in terms of weight loss and heat flow for *P*-Me-DNPT, *P*-OMe-DNPT and *P*-NH_2-DNPT, respectively. In case of *P*-Me-DNPT, the first predominant acoustic mode at 12.4 kHz has highest PA signal at T_d i.e. 250 ^oC as shown in Fig. 6(a). The compound starts releasing NO_2 at 90 ^oC and this temperature is treated as first thermal zone for release of NO_2. However, fixed intensity of acoustic modes shows the stability of compound between 90-170 ^oC range. The acoustic modes located at 8.5 and 22 kHz are also stable between 190-350 ^oC range.

Fig. 6(b) shows the heat flow curve of *P*-Me-DNPT, which confirms that the compound has melting temperature at 129.80 ^{o}C and decomposition temperature at 259.89 ^{o}C. The weight loss curve shows that the compound is thermally stable upto 150 ^{o}C and after crossing this temperature, the compound lost 95 % of its total weight at 233.48 ^{o}C. Therefore, strength of the PA signal and TG-DTA thermo graphs confirm that the *P*-Me-DNPT is thermally stable.

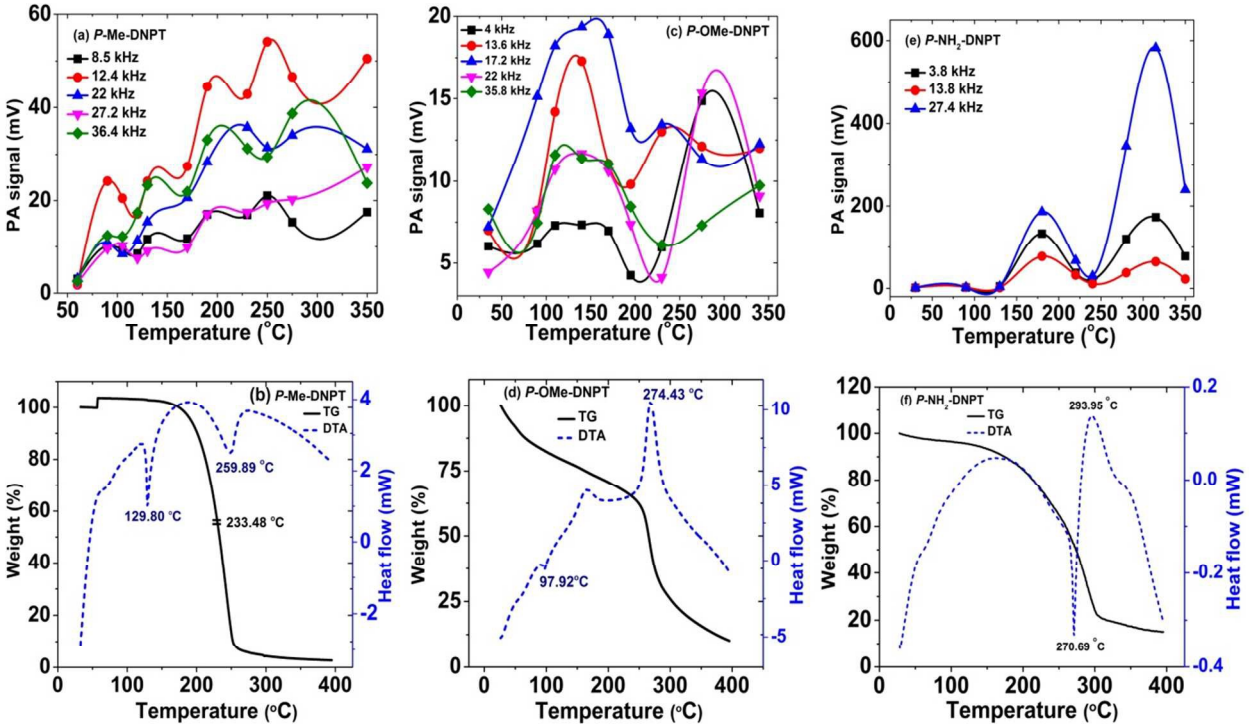

Fig. 6 Behavior of acoustic modes vs temperature and TG-DTA curves.

Fig. 6(c) shows the behavior of acoustic modes of *P*-OMe-DNPT with respect to temperature. The acoustic mode present at 17.2 kHz is one of the strongest PA mode between 90 and 195 ^{o}C temperature range. Similarly, modes present at 13.6 kHz show highest PA peak at 140 and 230 ^{o}C, while mode at 17.2 kHz has higher peak at 140 and 275 ^{o}C, respectively.

Fig. 6(d) shows the TG-DTA curves of *P*-OMe-DNPT, which has melting and decomposition temperatures at 97.92 and 274.43 ^{o}C, respectively. In addition, the heat flow curve shows the presence of broad peak at 175 ^{o}C between 150-180 ^{o}C, temperature range, which is also a decomposition point and correlated with strong PA signal due to release of more quantity of

NO_2. The weight loss curve shows gradual decay in the weight of the compound between 25-275 ^oC range. The rate of decomposition get accelerated after crosing 275 ^oC. It is also reflected in the strength of the PA signal of acoustic modes present at 4, 22 and 35.8 kHz which show stable behavior upto 275 ^oC.

Fig. 6(e) shows the behavior of three excited acoustic modes present at 3.8, 13.8 and 27.4 kHz, respectively. They show similar excitation behavior and the intensities of PA spectra shows two major peaks at 180 and 315 ^oC, respectively. The compound *P*-NH_2-DNPT is thermally stable upto 130 ^oC. Fig. 6(f), the heat flow curve of TG-DTA shows that the process of melting initiates at 180 ^oC and is completed at 270 ^oC, which is follwed by decomposition at 293 ^oC. The weight loss curve shows that compound is thermally stable upto 150 ^oC after this it losses around 70 % of its total weight between 150-300 ^oC range. But, the signature peak of PA signal appears at 130 ^oC which shows rapid growth up to 180 ^oC. The PA signal shows two additional peaks at 315 ^oC and 280 ^oC, respectively. The result obtained from of PA technique has excellent agrement with the TG-DTA analysis. The *P*-NH_2-DNPT has an additional N (due to -NH_2) which increases the density of compound (1.66 g/cm^3) as compared to other compounds and leads to releases more quantity of NO_2 than other gaseous molecules. Therefore, the synthesis of nitrogen (N) rich green energetic materials can be treated as a potential rocket fuels [2,3].

The heat of decomposition (ΔH) depends on the overall decomposition and type of byproducts formed. The ring breaks down reactions in process of thermal decomposition are either exothermic or endothermic in nature. The endothermic peak represents the solid–solid phase-transition points which releases condensed water. It is observed that in case of *P*-Me-DNPT, at decomposition temperature (259 ^oC), the heat flow curve shows endothermic peak (Fig. 6(b)), whereas the weight loss curve indicates that almost 95 % weight is lost between 150-260

^{o}C range. This shows that the molecule start decomposing at 259 ^{o}C, by releasing different types of gaseous byproducts along with condensed water (which is due to lack of high nitrogen content). Consequently, it shows endothermic peak for *P*-Me-DNPT [34]. However, *P*-OMe-DNPT and *P*-NH_2-DNPT are oxygen and nitrogen rich compounds. As a result at decomposition temperature the ring-breaking reaction appears in form of exothermic peaks (due to oxidation of nitrogen) as shown in Fig. 6 (d) and (f), respectively. *P*-OMe-DNPT shows two exothermic peaks at 150 ^{o}C and 274.43 ^{o}C, respectively. The first exothermic peak is due to breaking of principal functional groups attached to the ring, while the second one is due to concerted ring breaking mechanism and indicates completion of total decomposition process.

3.4. Effect of incident laser energy (E_{in})

Fig. 7(a-f) shows the PA spectra of 1, 2, 4-triazole compounds and the corresponding behavior of the acoustic modes with respect to incident laser energy. The thermal PA spectra of the compounds are recorded at E_{in} = 8.63 mJ. We have studied the effect of incident laser energy on PA signal after crossing the T_d, and recorded the threshold value of incident laser energy required to generate the PA signal.

The PA spectra of *P*-Me-DNPT at E_{in} = 7.86 mJ shows well-distinguished and sharp acoustic modes as compared to 6.3 mJ. While, in case of *P*-OMe-DNPT 5.25 mJ energy is sufficient enough to generate the strong PA signal which confirms that it releases more quantity of gaseous products than the *P*-Me-DNPT. Thus, the experimental findings support that the release mechanism of NO_2 along with other byproduct gaseous molecules are purely dependent on the structures of the compounds and location of functional group at *para* position of phenyl ring of 1,2,4-triazoles. However, the compound *P*-NH_2-DNPT initiates the release of NO_2 after crossing the

temperature 130 ^{o}C, which is also reflected in terms of PA signal. Therefore, *P*-NH_2-DNPT needs small value of incident laser energy which is sufficient enough to generate the strong PA signal.

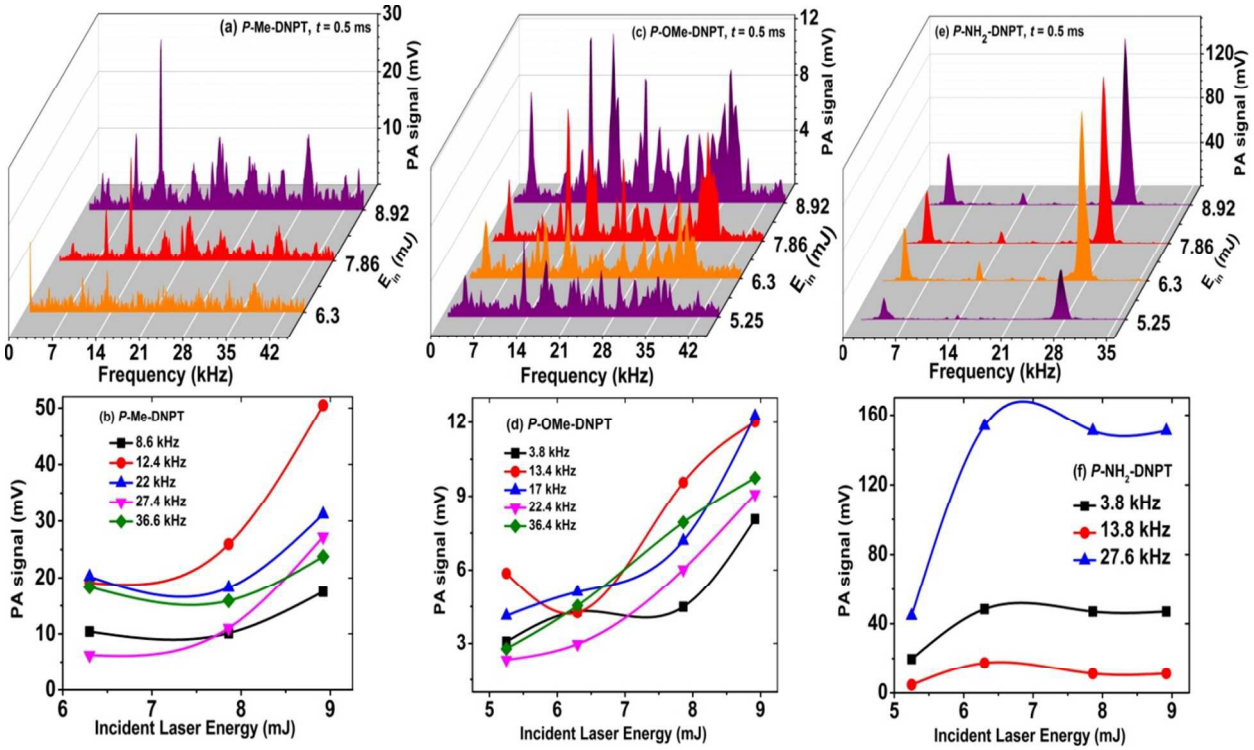

Fig. 7 PA spectra and behavior of acoustic modes with respect to incident laser energy.

The PA results also show that the phenyl series 1,2,4-triazoles require high incident laser energy as compared to the previously reported benzyl series of 1,2,3-triazoles [31,35]. Since, phenyl series compounds have direct bonding between two aromatic rings i.e. 1,2,4-triazole moiety and phenyl ring, respectively. Consequently, this series compounds release low quantity of gaseous products. However, in case of benzyl series, 1,2,3-triazole moiety is connected to phenyl ring through -CH_2 group. Thus during thermal decomposition process of benzyl series 1,2,3- triazoles releases more quantity of gaseous fragments than the phenyl series 1,2,4- triazoles. Therefore, they need low incident laser energy to generate strong PA signal.

3.5. Effect of data acquisition time (*t*)

The acoustic wave activation time is controlled by the data acquisition time through the oscilloscope. Therefore, the PA spectra at different data acquisition times provide the detailed

information about the behavior of acoustic modes with respect to different time frame. Fig. 8(a-f) shows the PA spectra and decay behavior of acoustic modes with respect to data acquisition time for *P*-Me-DNPT, *P*-OMe-DNPT, and *P*-NH_2-DNPT, respectively. The PA spectra are recorded at decomposition temperature and E_{in} = 8.63 mJ. The excited acoustic modes located at 22, 13.8 and 4 kHz have their corresponding decay times of the order of 0.43, 0.26, and 0.25 ms respectively. For *P*-NH_2-DNPT, the decay time of acoustic modes are lower than the other compounds. This clearly indicates that the compound which have high concentration of NO_2 molecules possess lower decay time due to short collision time.

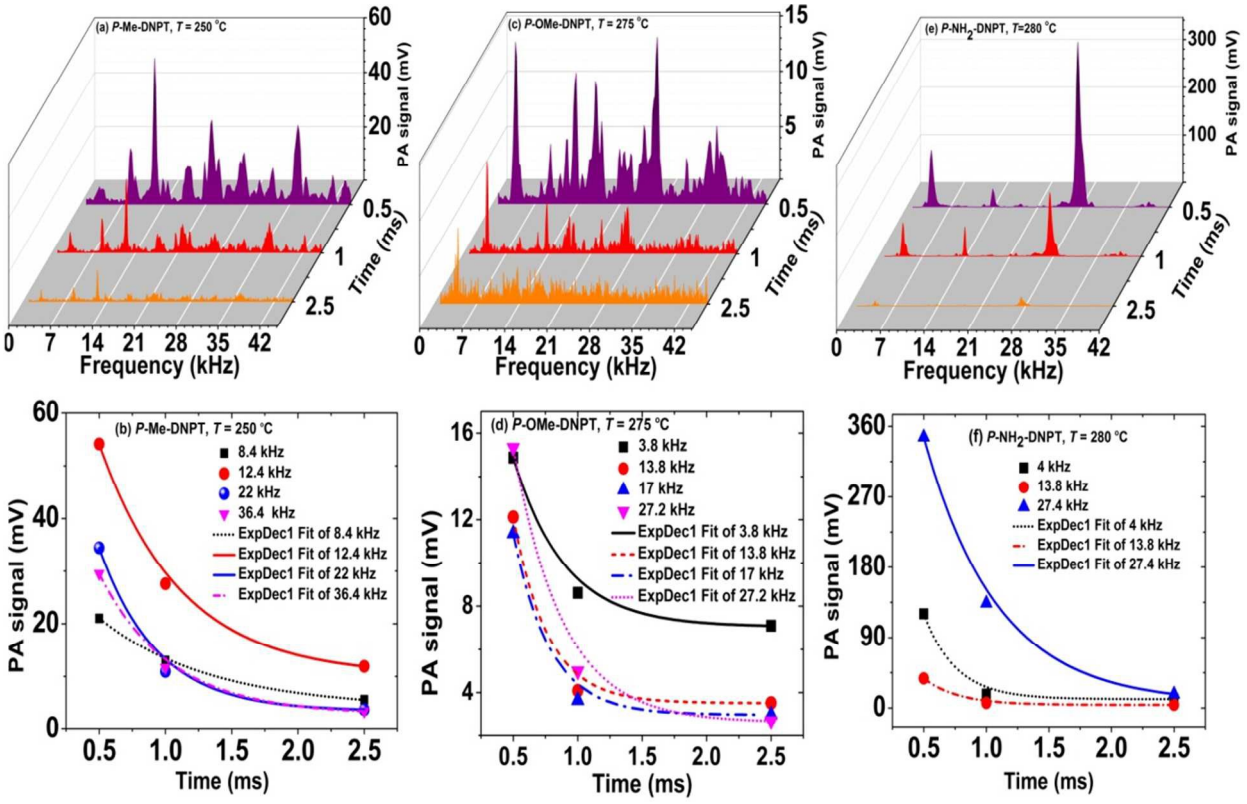

Fig. 8 PA spectra and behavior of acoustic modes with data acquisition time.

It is also observed that at t = 2.5 ms the magnitude of excited acoustic modes of *P*-OMe-DNPT become minimum and provides weak PA signal. Therefore, according to kinetic theory of gases the selection of lower time scales i.e. $t \leq 1$ ms is most suitable for recording the PA signal for

trace level detection of gaseous products. Since, all the excited acoustic modes show exponential decay behavior with different decay times. Therefore, selection of t = 0.5 ms provides the strong PA signal of high resolution as compared to the other time scales.

3.6. Bond breaking mechanism and scaling the efficiency of compounds as a rocket fuel

The sequence of bond breaking mechanisms of major functional groups from solid compound during the pyrolysis process is explained in terms of their bond lengths. The bond length of the compounds are calculated by optimizing the structure in Gaussian 03 program using B3PW91 functional with 6-31G(d,p) basis set [21]. The bond lengths of principal functional groups are listed in Table. 1.

Table. 1 Bond lengths of compounds and PA signal at t = 0.5 ms.

Functional groups	*P*-Me-DNPT	*P*-OMe-DNPT	*P*-NH_2-DNPT
C_{phenyl} - $N_{triazole}$	1.407 Å	1.412 Å	1.410 Å
C_{phenyl} – *para* group	1.503 Å (C-CH_3)	1.345 Å (C-OCH_3)	1.330 Å (C-NH_2)
-C-NO_2	1.474 Å	1.476 Å	1.450 Å
Strength of PA signal	54.11 mV	19.36 mV	582.99 mV

In case of *P*-Me-DNPT, the methyl group is present at *para* position of phenyl ring with sigma bond which has bond length of the order of 1.503 Å. In addition, two NO_2 groups which are attached in 3,5 (*meta*)-positions of phenyl ring with sigma bond which has the bond length of the order of 1.474 Å. Since, the bond length of *para* position methyl group is higher than the nitro groups. Therefore, the supplied heat energy during pyrolysis was first used to cease the methyl group followed by the nitro group and then triazole group, respectively. As a result, less quantity of NO_2 molecules are released. While, for *P*-NH_2-DNPT the bond length between *para* position amino group to phenyl ring is 1.330 Å, and the bond length between meta nitro groups to phenyl ring is 1.450 Å. In this case, the supplied heat energy at initial level is utilized to cease the nitro

groups from the phenyl ring rather than amino group. Consequently, high yield of NO_2 molecules are released which leads to generation of the strongest PA signal of the order of 582.99 mV. Similarly, in case of *P*-OMe-DNPT, the bond length between *para* methoxy group to phenyl ring is 1.345 Å, and the bond length of nitro group to phenyl ring is of the order of 1.476 Å. Therefore, decomposition process initiates with release of NO_2 molecules and followed by methoxy group fragmentation. Further, $-OCH_3$ group is defragmented into O, CO, H_2, H_2O .etc. It appears that the concentration of either of these fragments are equally high along with NO_2 in the gas mixture which has no absorption in 532 nm range. Therefore, the acoustic modes possess pair of peaks and have low strength PA signal for *P*-OMe-DNPT, even though, *P*-OMe-DNPT initially releases high quantity of NO_2 along with other gaseous molecules. The strength of the PA signal is only monitered in terms of NO_2 concentration. Whereas, presence of other gases leads to broadening of the profile of acoustic modes along with the shift from actual calculated values of modes.

The rupture of single bond (C-N) molecules requires lower energy than the double bond (N=N) molecules. This is because, the double bonded molecules have higher bond strengths. Therefore, the process of decomposition of reported 1,2,4-triazoles is completed in two steps. In first step, the triazole moeity is seperated from the phenyl ring and the final step follows with concerted ring breaking. The aromatic ring like triazole moeity requires high energy than the aliphatic groups such as $-CH_3$, $-OCH_3$ and $-NH_2$ for seperation from the ring. The entire molecules along with their principal functional groups are decomposed easily at high temperature. However, during the pyrolysis of HEMs compounds between 30-350 ^oC range release their fragments and higher concentration of gaseous products at T_m, T_d, and after crossing the T_d. Which shows that the thermal stability of compounds. The expected order of ceased

functional groups from the ring during the process of decomposition with respect to the supplied heat energy is listed in Table. 2.

Table. 2 The expected order of ceased functional groups during pyrolysis based on bond lenghts.

Compound	Order
P-Me-DNPT	$-CH_3$, $-NO_2$, -triazole
P-OMe-DNPT	$-NO_2$, -triazole, $-OCH_3$
P-NH_2-DNPT	$-NO_2$, -triazole, $-NH_2$

The decomposition mechanism might be more complex and it may involve bond rearrangements and isomerizations before fragmentation or decomposition. However, the order of ceased functional groups can be confirmed on the basis of PA spectra of compounds in terms of their excited acoustic modes and intensity of PA signal.

The estimated percentile residual quantity of compound from weight loss curve at 400 ^oC for *P*-Me-DNPT: 3 % (Initial wieght (I_w): 1.589 mg) , *P*-OMe-DNPT: 10 % (I_w: 1.002 mg) and *P*-NH_2-DNPT: 15 % (I_w: 3.254 mg). The highest PA signal obtained for this succesive compound at t = 0.5 ms and are given by 54.11, 19.36 and 582.99 mV. While, for t = 1 ms, the strength of the signal is of the order of 30.08, 9.7 and 36.12 mV, respectively. Even though the initial weight of *P*-OMe-DNPT is less, but it show comparatively high residual weight and lower strength of the PA signal than other the two compounds. Therefore, on the basis of the residual weight from TG-DTA and the obtained strength of the PA signal the efficiency of these compounds as a rocket fuel is found in the sequence of *P*-NH_2-DNPT > *P*-Me-DNPT > *P*-OMe-DNPT, respectively. The similar order is applicable for explosive properties of these compounds. The efficiency of these compounds as a rocket fuel is ascertained on the basis of released quantity of NO_2 molecules in temrs of strength of PA signal. Because, NO_2 is identified as freely released gas during the pyrolysis of HEMs which is treated as a thermal marker [29,30,31].

3.7. Comparisons between GC-MS and PA techniques

The Gas chromatography mass spectroscopy (GC-MS) is a well known analytical technique which is used for solid, liquid and gases. It works on the principle of column seperation for which the solid sample is required to be dissolved in a perticular solvent. Moreover, entire process starts above 200 ^{o}C of oven. The solid compound heated upto required temperature and introduced to oven along with injector (N_2 or He). Then after measured the individual concentrations of each gas composition based on their column condition and the retension time. However, the PA pyrolysis technique is a simple non distructive in nature which does not require sample preparation and need very small quantity of solid samples. Here, excitation laser wavelength is selected according to the absorption characteristics of released gas (for our case NO_2) from the solid compound. In addition, it does not required any purge gas. The PA signal is produced due to non radiative transition which is detected by a prepolarized microphone. This is treated as one of the most sensitive detection technique and have low level detection limit of the order of ppb. The GC-MS requires vapor minimum pressure of the order of 10 Torr, whereas PA technique needs vapor even less than 1 Torr. Furthermore, the controlled pyrolysis of the compound helps us to monitor the release of NO_2 gas at different temperatures. Apart from NO_2 other gaseous components can also be identified by the selection of tunable laser wavelengths.

Unlike GC-MS, the present form of PA technique is based on 532 nm wavelength is not able to monitor the individual concentrations of byproduct gaseous molecules released from HEMs during the thermal decomposition process. However, we can monitor the release of NO_2 below the melting temperature to study the thermal stability of the compound. Also, the change in the density of vapor is observed in terms of shift in the frequency of acoustic modes.

4. Conclusions

We have successfully recorded the thermal PA spectra of the newly synthesized 1,2,4-triazoles. The role of the bond breaking mechanism of principal functional groups during thermal decomposition process between 30 and 350 ^{o}C range, has been examined in terms of their bond lengths. The thermal stability of these compounds explained based on strength of PA signal and TG-DTA analysis. In addition, the efficiency of these compounds as rocket fuel for military applications, explosives have been investigated and found in given order *P*-NH_2-DNPT > *P*-Me-DNPT > *P*-OMe-DNPT. The effect of incident laser energy and data acquisition time on PA signal of the compounds is also studied. The study reveals that the compound *P*-NH_2-DNPT requires less incident laser energy as compared to other compounds. In case of reported phenyl series 1,2,4-triazoles $t \leq 1$ ms is the suitable data acquisition time to record their thermal photoacoustic fingerprint spectra.

Acknowledgements The authors gratefully acknowledge the D.R.D.O., Ministry of Defence, Govt. of India, India, for financial support. Our thanks are due to Dr. K.V. Rao, Director, ACRHEM, University of Hyderabad, for moral encouragement and keen interest.

References

1. Q. Wu, W. Zhu, and H. Xiao, *RSC Adv.*, 2014, **4**, 53000–53009.

2. D. Srinivas, V. D. Ghule, and K. Muralidharan, *RSC Adv.*, 2014, **4**, 7041–7051.

3. A. S. Kumar, V. D. Ghule, S. Subrahmanyam, and A. K. Sahoo, *Chemistry*, 2013, **19**, 509–18.

4. Y. Zhang, D. A. Parrish, and J. M. Shreeve, *J. Mater. Chem. A*, 2013, **1**, 585–593.

5. N. Fischer, D. Fischer, T. M. Klapötke, D. G. Piercey, and J. Stierstorfer, *J. Mater. Chem.*, 2012, **22**, 20418.

6. T. M. Klapötke and C. M. Sabaté, *Chem. Mater.*, 2008, **20**, 3629–3637.

7. H. S. Jadhav, M. B. Talawar, R. Sivabalan, D. D. Dhavale, S. N. Asthana, and V. N. Krishnamurthy, *J. Hazard. Mater.*, 2007, **143**, 192–197.

8. P. Zhang, S. J. Klippenstein, L. B. Harding, H. Sun, and C. K. Law, *RSC Adv.*, 2014, **4**, 62951–62964.

9. T. M. Klapo, P. Mayer, A. Schulz, and J. J. Weigand, *J. Am. Chem. Soc.*, 2005, **127**, 2032–2033.

10. X. Liu, Q. Yang, Z. Su, S. Chen, G. Xie, Q. Wei, and S. Gao, *RSC Adv.*, 2014, **4**, 16087–16093.

11. V. Kraft, W. Weber, M. Grutzke, M. Winter, and S. Nowak, *RSC Adv.*, 2015, **5**, 80150–80157.

12. J. Cheng, R. Zhang, Z. Liu, L. Li, F. Zhao, and S. Xu, *RSC Adv.*, 2015, **5**, 50278–50288.

13. R. Turcotte, M. Vachon, Q. S. M. Kwok, R. Wang, and D. E. G. Jones, *Thermochim. Acta*, 2005, **433**, 105–115.

14. M. F. Foltz, C. L. Coon, F. Garcia, and A. L. Nichols III, *Propellants, Explos. Pyrotech.*, 1994, **19**, 133–144.

15. D. E. G. Jones, P. D. Lightfoot, R. C. Fouchard, Q. Kwok, A. M. Turcotte, and W. Ridley, *Thermochim. Acta*, 2002, **384**, 57–69.

16. S. T. L. H. Frans J.M. Harren, Gina Cotti, Jos Oomens, *Encycl. Anal. Chem.*, 2000, 2203–2226.

17. S. Schäfer, M. Mashni, J. Sneider, and A. Mikl, *Appl. Phys. B*, 1998, **66**, 511–516.

18. M. S. Churio, M. a. Brusa, M. a. Grela, S. G. Bertolotti, and C. M. Previtali, *Phys. Chem. Chem. Phys.*, 2003, **5**, 902.

19. C. L. Spencer, V. Watson, and M. Hippler, *Analyst*, 2012, **137**, 1384.

20. J. W. Lu, J. M. Flores, A. Lavi, A. Abo-Riziq, and Y. Rudich, *Phys. Chem. Chem. Phys.*, 2011, **13**, 6484.

21. N. Kommu, V. D. Ghule, A. S. Kumar, and A. K. Sahoo, *Chem. Asian J.*, 2014, **9**, 166–78.

22. J. A. Conkling, *Propellants*, Scientific American, Second Edi., 1996.

23. A. Miklós, P. Hess, and Z. Bozóki, *Rev. Sci. Instrum.*, 2001, **72**, 1937–1955.

24. F. Yehya and A. K. Chaudhary, *J. Mod. Phys.*, 2011, **02**, 200–209.

25. R. Bartlome, M. Kaučikas, and M. W. Sigrist, *Appl. Phys. B Lasers Opt.*, 2009, **96**, 561–566.

26. F. Yehya and A. K. Chaudhary, *Opt. Commun.*, 2014, **312**, 16–22.

27. L. Y. Hao, J. X. Han, Q. Shi, J. H. Zhang, J. J. Zheng, and Q. S. Zhu, *Rev. Sci. Instrum.*, 2014, **1975**, 1–7.

28. L. Krämer, Z. Bozoki, and R. Niessner, *Anal. Sci.*, 2001, **17**, 563–566.

29. F. Yehya and A. K. Chaudhary, *Sensors Actuators B. Chem.*, 2013, **178**, 324–330.

30. F. Yehya and A. K. Chaudhary, *Appl. Phys. B*, 2012, **110**, 15–22.

31. K. S. Rao, F. Yehya, A. K. Chaudhary, A. S. Kumar, and A. K. Sahoo, *J. Anal. Appl. Pyrolysis*, 2014, **109**, 132–139.

32. P. J. Crutzen and M. Oppenheimer, *Clim. Change*, 2008, **89**, 143–154.

33. A. Burcat and A. Lifshitz, *J. Phys. Chem.*, 1970, **74**, 263–268.

34. A. S. Kumar, N. Kommu, V. D. Ghule, and A. K. Sahoo, *J. Mater. Chem. A*, 2014, **2**, 7917.

35. K. S. Rao and A. K. Chaudhary, *Thermochim. Acta*, 2015, **614**, 149–156.